

# Journal of Materials Chemistry A

Accepted Manuscript



This is an *Accepted Manuscript*, which has been through the Royal Society of Chemistry peer review process and has been accepted for publication.

*Accepted Manuscripts* are published online shortly after acceptance, before technical editing, formatting and proof reading. Using this free service, authors can make their results available to the community, in citable form, before we publish the edited article. We will replace this *Accepted Manuscript* with the edited and formatted *Advance Article* as soon as it is available.

You can find more information about *Accepted Manuscripts* in the [Information for Authors](#).

Please note that technical editing may introduce minor changes to the text and/or graphics, which may alter content. The journal's standard [Terms & Conditions](#) and the [Ethical guidelines](#) still apply. In no event shall the Royal Society of Chemistry be held responsible for any errors or omissions in this *Accepted Manuscript* or any consequences arising from the use of any information it contains.

## ARTICLE

# Point defect-assisted doping mechanism and related thermoelectric transport properties in Pb-doped BiCuOTe

Cite this: DOI: 10.1039/x0xx00000x

Received 00th January 2012,  
Accepted 00th January 2012

DOI: 10.1039/x0xx00000x

www.rsc.org/

Tae-Ho An,<sup>a,b</sup> Young Soo Lim,<sup>\*a</sup> Hyoung-Seuk Choi,<sup>a</sup> Won-Seon Seo,<sup>a</sup> Cheol-Hee Park,<sup>c</sup> Gwi-Rang Kim,<sup>b</sup> Chan Park,<sup>\*b</sup> Chang Hoon Lee<sup>d</sup> and Ji Hoon Shim<sup>\*d,e</sup>

We report point defect-assisted doping mechanism and related thermoelectric transport properties in Pb-doped BiCuOTe compounds. The substitution of trivalent Bi<sup>3+</sup> with divalent Pb<sup>2+</sup> led to the generation of more than one hole per single Pb atom. The origin of the extra charge carrier was discussed in terms of the formation energy of *p*-type native point defects, and it could be evidenced by the density functional theory calculations. Related charge transport properties indicated that control of the native point defect is critical to achieve high thermoelectric performance in BiCuOTe material system.

## Introduction

Recently, BiCuO $Q$  ( $Q$  = chalcogen) oxychalcogenides have attracted much attention as promising thermoelectric materials for power generation using waste heat. It has a ZrCuSiAs type structure (space group = P4/nmm) and consists of alternately stacked (Bi<sub>2</sub>O<sub>2</sub>)<sup>2+</sup> insulating layers and (Cu<sub>2</sub>Q<sub>2</sub>)<sup>2-</sup> conducting layers along the *c*-axis.<sup>1-3</sup> It exhibits extremely low lattice thermal conductivity ( $\kappa_{\text{ph}} < 1.0 \text{ Wm}^{-1}\text{K}^{-1}$ ),<sup>4-6</sup> while the electrical conductivity ( $\sigma$ ) of BiCuO $Q$ , whose valence band minima is comprised of Cu 3*d* and  $Q$  *p*, is relatively poor due to its low hole mobility.<sup>7-11</sup> The electrical conductivity, however, can be significantly improved by doping of various elements (Mg<sup>2+</sup>, Ca<sup>2+</sup>, Sr<sup>2+</sup>, Ba<sup>2+</sup>, Pb<sup>2+</sup>, Na<sup>+</sup>, and K<sup>+</sup>), which can lead to the remarkable enhancement of thermoelectric performance.<sup>4,5,6,12-20</sup> We reported the simultaneous increase in both the carrier concentration and the mobility in K-doped BiCuOSe compounds, and its origin was discussed in terms of the two-band structure of BiCuOSe.<sup>20</sup> Sui *et al.* reported the highest thermoelectric figure-of-merit  $ZT$  ( $= S^2\sigma T/\kappa$ , where  $S$  is Seebeck coefficient,  $\kappa$  is thermal conductivity and  $T$  is absolute temperature) of 1.4 at 923K in textured Ba-doped BiCuOSe,<sup>15</sup> and it was superior to the state-of-the-art  $ZT$  value reported in *p*-type skutterudite system ( $ZT = 1.2$  at 800K).<sup>21</sup>

Compared with other thermoelectric materials, the achieved high thermoelectric performance of BiCuOSe mainly originates from its very low thermal conductivity rather than its power factor. Actually, the power factors ( $PF = S^2\sigma$ ) of BiCuOSe ( $< 1 \times 10^{-3} \text{ Wcm}^{-1}\text{K}^{-2}$ )<sup>4,5,6,12-20</sup> were reported to be considerably smaller than that of the *p*-type skutterudite ( $> 4.5 \times 10^{-3} \text{ Wcm}^{-1}\text{K}^{-2}$ ).<sup>21</sup> In this respect, BiCuOTe is one of the suitable

thermoelectric materials to obtain high power factor in BiCuO $Q$  system. Because the antibonding of Cu 3*d*-Te 5*p* state is stronger than Cu 3*d*-Se 4*p* states at same doping level, the hole mobility can be significantly improved in BiCuOTe.<sup>22</sup> Therefore, the power factors in undoped BiCuOTe are superior to that in undoped BiCuOSe, leading to high  $ZT$  (0.66 at 673K)<sup>23</sup> compared with that in the undoped BiCuOSe ( $\sim 0.4$  at 673K).<sup>4,5,6,12-20</sup> However, contrary to the case of BiCuOSe, the carrier optimization for the improvement of  $ZT$  by the impurity doping has not been successful in BiCuOTe. The electrical conductivity could be enhanced by Pb-doping in the BiCuOTe, while the power factors were not significantly improved due to the drastic reduction in Seebeck coefficient. To make matters worse, the strengthened electrical contribution to the thermal conductivity ( $\kappa_{\text{hole}}$ ) by Pb-doping leads to the decrease of  $ZT$  values.<sup>23</sup> Therefore, understanding the effect of doping on the thermoelectric properties is of great significance for the enhancement of thermoelectric performance of BiCuOTe.

In this work, point defect-assisted doping mechanism and related thermoelectric transport properties in Pb-doped BiCuOTe compounds are presented. Even undoped BiCuOTe compound exhibited degenerately doped semiconducting behaviour up to extrinsic-intrinsic transition temperature, and this result indicates that native point defects are the main source of the hole generation in BiCuOTe. Hole concentration increased with the increase in the amount of the Pb, resulting in the significant increase in the electrical conductivity of Pb-doped BiCuOTe. However, although at most one hole per single dopant atom could be generated due to the divalency of Pb, more than one hole per a Pb atom were generated in the Pb-doped compound. The dependence of the formation energies of

possible point defects ( $V_{\text{Cu}}$  and  $V_{\text{Bi}}$ ) on the amount of Pb-doping were calculated based on density functional theory (DFT), and the results were quite consistent with our observations. Details in the thermoelectric transport properties of the Pb-doped BiCuOTe compounds were also discussed.

## Experimental

$\text{Bi}_{1-x}\text{Pb}_x\text{CuOTe}$  ( $x = 0, 0.01, 0.02, 0.04$  and  $0.06$ ) compounds were synthesized by one step solid state reaction.  $\text{Bi}_2\text{O}_3$  (99.999%, Sigma Aldrich), Bi (99.999 %, 5N Plus), Te (99.999 %, 5N Plus), Cu (99.99%, Alfa Aesar) and Pb (99.9%, Alfa Aesar) were used as starting materials. Mixtures of starting materials were ground with an alumina mortar and pestle, and they were pressed into pellets under uniaxial stress (80 MPa). The pressed pellets were annealed at 788K for 12 h in evacuated silica tubes to obtain a homogeneous BiCuOTe phase. The annealed samples were pulverized into powders, and then the powders were consolidated by spark plasma sintering at 748K under 50 MPa of pressure for 5 min in a  $10^{-3}$  Torr vacuum. Phase analyses of the compounds were performed using an X-ray diffractometer (XRD, New D8 Advance, Bruker). Electrical conductivities and Seebeck coefficients were measured by a thermoelectric property measurement system (TPMS, RZ-2001i, Ozawa Science), and carrier concentration and mobility were determined using a Hall measurement system (Hall, ResiTest 8300, Toyo Corporation).

The crystal structure optimization for the Pb-doped BiCuOTe compound was carried out using a set of 200 k-points for the irreducible Brillouin zone. Calculation of vacancy formation energy for Pb-doped and undoped case and calculation of the change of lattice parameter as a function of Pb-doping concentration were also performed. In the calculation, a set of 200 k-points for the irreducible Brillouin zone was used, and the self-consistent-field convergence thresholds were  $10^{-5}$  eV and  $0.001$  eV/Å for the total electronic energy and force, respectively. The DFT calculations employed the frozen-core projector augmented wave (PAW) method<sup>24,25</sup> encoded in the Vienna *ab initio* simulation package (VASP).<sup>26</sup> The generalized-gradient approximation (GGA)<sup>27</sup> of Perdew, Burke and Ernzerhof (PBE) was used for the exchange-correlation functional with the plane-wave-cut-off energy of 550 eV.

## Results and discussion

Figure 1(a) shows XRD patterns of the as-prepared  $\text{Bi}_{1-x}\text{Pb}_x\text{CuOTe}$  ( $x = 0, 0.01, 0.02, 0.04$  and  $0.06$ ) compounds. The XRD patterns indicate that the compounds consist of a single phase of BiCuOTe with little trace of  $\text{Bi}_2\text{O}_3$  secondary phase. The formation of  $\text{Bi}_2\text{O}_3$  secondary phase was not affected by the amount of Pb-doping, and it was evidenced by the peak-to-peak height between the  $\text{Bi}_2\text{O}_3$  and BiCuOTe phase (Figure S1). As shown in Figure 1(b), the lattice parameters along  $a$ - and  $c$ -axis increased with the increase in the amount of Pb as summarized in Table 1. Standard deviations of the lattice parameters are provided in Table S1. The increase of the lattice

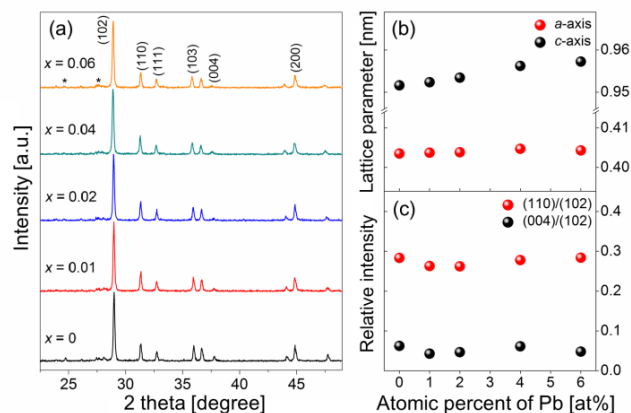


Fig. 1(a) X-ray diffraction patterns of the  $\text{Bi}_{1-x}\text{Pb}_x\text{CuOTe}$  compounds. (b) Dependence of the lattice parameters on the amounts of Pb-doping and (c) relative intensities of (110) to (102) and (004) to (102) peaks in the XRD patterns.

parameter is due to the ionic radius of  $\text{Pb}^{2+}$  (0.129 nm) which is larger than that of  $\text{Bi}^{3+}$  (0.117 nm).<sup>28</sup> The increase of the lattice parameter along the  $c$ -axis is more significant than that along the  $a$ -axis, and the calculated values based on DFT calculations also exhibited the same tendency. This behaviour can be related with the decrease in the columbic attraction between  $(\text{Bi}_2\text{O}_2)^{2+}$  insulating layers and  $(\text{Cu}_2\text{O}_2)^{2-}$  conducting layer as proposed by Barreteau *et al.*<sup>32</sup> Figure 1(c) presents the relative intensities of (004) to (102) and (110) to (102) peaks in the XRD patterns. Because the relative intensities were not strongly dependent on the amount of Pb-doping, it is possible to compare the following thermoelectric transport properties directly without further consideration on the additional effects of the microstructure.

Figure 2(a) shows temperature-dependent electrical conductivities of the  $\text{Bi}_{1-x}\text{Pb}_x\text{CuOTe}$  compounds. The electrical conductivities of the compounds increased with the increase in the amount of Pb-doping, indicating that the Pb atom is an effective acceptor for BiCuOTe. The electrical conductivities of Pb-doped compounds decreased with the increase in temperature. As shown in the inset, the electrical conductivities were proportional to  $T^{-1.5}$  at relatively low temperature, which indicates that the hole-acoustic phonon scattering is the dominant mechanism for the metallic conduction behaviour in

Table 1. Experimental (Exp.) and calculated (Calc.) lattice parameters along  $a$ - and  $c$ -axis.

Pb (at%)	$a$ (nm)		$c$ (nm)	
	Exp.	Calc.	Exp.	Calc.
0	0.4035	0.4058	0.9516	0.9724
1	0.4037	0.4059	0.9524	0.9742
2	0.4039	0.4060	0.9534	0.9752
4	0.4047	0.4061	0.9562	0.9765
6	0.4043	0.4061	0.9572	0.9783

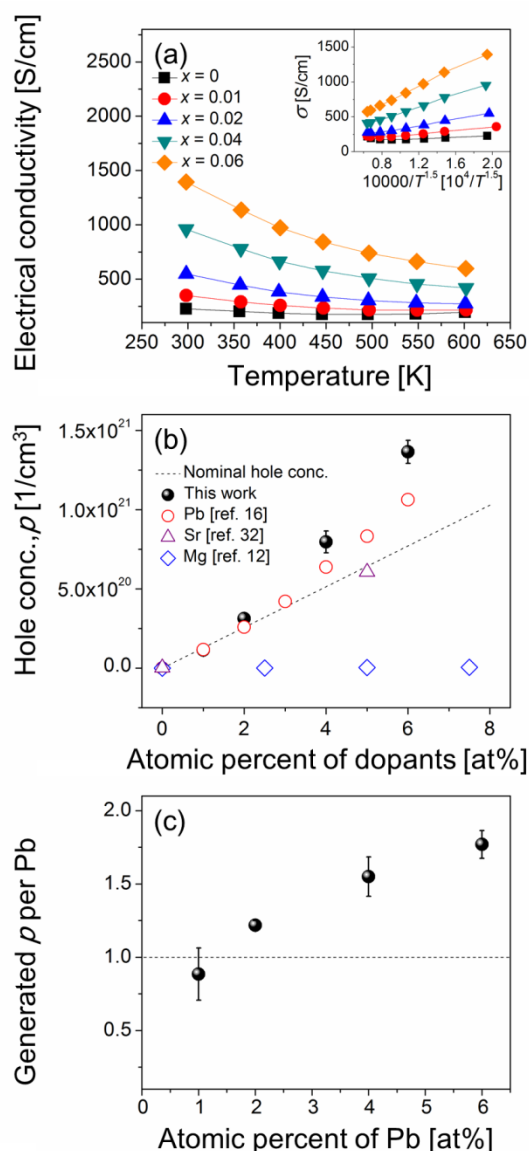


Fig. 2(a) Temperature-dependent electrical conductivities of the  $\text{Bi}_{1-x}\text{Pb}_x\text{CuOTe}$  compounds. A plot of  $\sigma$  vs.  $10000/T^{1.5}$  is shown in the inset. (b) Dependence of carrier concentration on the atomic percent of dopants in the  $\text{BiCuOTe}$  (filled) and  $\text{BiCuOSe}$  compounds (open). (c) Hole generation per a Pb atom (doping yield) as a function of the atomic percent of Pb in the  $\text{Bi}_{1-x}\text{Pb}_x\text{CuOTe}$  compounds.

$\text{BiCuOTe}$  at this temperature range. The temperature dependence of  $T^{-1.5}$  was much obvious in the compounds with relatively high Pb content ( $x \geq 0.04$ ), indicating that these compounds are degenerately doped in the whole temperature range used in this study. In the case of  $x \leq 0.02$ , the electrical conductivity was no longer linearly proportional to  $T^{-1.5}$  at relatively high temperature due to the extrinsic-intrinsic transition.

To understand the effect of Pb-doping on the electrical conductivity, Hall measurements of the compounds were performed at room temperature. As shown in Table 2, the

electrical conductivities characterized by TPMS ( $\sigma_{\text{TPMS}}$ ) were in reasonably good agreement with those by Hall measurements ( $\sigma_{\text{Hall}}$ ). Figure 2(b) presents hole concentrations at room temperature as a function of the amount of Pb-doping in the  $\text{Bi}_{1-x}\text{Pb}_x\text{CuOTe}$  compounds. The hole concentration increased with the increase in the amount of Pb, and the value in 6 at% Pb-doped  $\text{BiCuOTe}$  compound ( $1.4 \times 10^{21} \text{ cm}^{-3}$ ) was more than one order higher than that in the undoped compound ( $6.9 \times 10^{19} \text{ cm}^{-3}$ ). The doping mechanism can be simply explained by the substitution of  $\text{Bi}^{3+}$  by  $\text{Pb}^{2+}$  as same as in Pb-doped  $\text{BiCuOSe}$  compounds.<sup>16-18</sup> The  $\text{Bi}^{3+}$  substitution with  $\text{Pb}^{2+}$  results in the generation of hole carriers in the insulating layer of  $[\text{Bi}_2\text{O}_2]^{2+}$ , and then the holes are transferred into the conducting layer of  $[\text{Cu}_2\text{Se}_2]^{2-}$  in the Pb-doped  $\text{BiCuOTe}$  compounds. However, it is noteworthy that the carrier concentrations in the Pb-doped compounds are higher than the nominal carrier concentration (indicated by dashed line; the case when a single dopant atom in the site of Bi provides only one hole through the mechanism described above). This tendency is much clearly observed in the compounds with high Pb content as shown in Figure 2(c).

This anomalous doping effect of Pb has also been reported in  $\text{BiCuOSe}$  compounds. Dopants whose ionic radii are larger than that of  $\text{Bi}^{3+}$  (0.117 nm), such as  $\text{Pb}^{2+}$  (0.133 nm) and  $\text{Sr}^{2+}$  (0.132 nm), have exhibited strong doping efficiency in this material system.<sup>16,32</sup> In contrast, the doping yield was far below unity in the case of  $\text{Mg}^{2+}$  (0.086 nm).<sup>12</sup> Actually, because a considerably high hole concentration ( $6.9 \times 10^{19} \text{ cm}^{-3}$ ) was observed even in the undoped compound, it is obvious that native point defects play an important role in this material system. Therefore, it can be reasonably proposed that the doping mechanism is closely related with the formation of extra point defects due to the existence of foreign ions in  $\text{Bi}^{3+}$  sites.

Meanwhile, the mobility continuously decreased with the increase in the amount of Pb as shown in Table 2 and Figure 3(a). In our previous report, it was revealed that the mobility is critically affected by the two-band structure in  $\text{BiCuOQ}$ .<sup>20</sup> The charge transport in undoped  $\text{BiCuOSe}$  ( $p = 5.1 \times 10^{18} \text{ cm}^{-3}$ ) was determined by heavy-hole band, while that in degenerately doped  $\text{BiCuOSe}$  ( $p = 2.3 \times 10^{19} \text{ cm}^{-3}$ ) was governed by light-hole band as schematically drawn in Figure 3(b). Therefore, it led to an abrupt increase in the mobility from 2.4 (undoped) to  $12.6 \text{ cm}^2\text{V}^{-1}\text{s}^{-1}$  (doped) by the increase in the hole concentration.

Table 2. Electrical conductivities characterized by TPMS and Hall, hole concentration ( $p$ ) and mobility ( $\mu$ ) at room temperature.

Pb (at%)	$\sigma_{\text{TPMS}}$ ( $\text{Scm}^{-1}$ )	$\sigma_{\text{Hall}}$ ( $\text{Scm}^{-1}$ )	$p$ ( $\text{cm}^{-3}$ )	$\mu$ ( $\text{cm}^2\text{V}^{-1}\text{s}^{-1}$ )
0	$2.3 \times 10^2$	$1.4 \times 10^2$	$6.9 \times 10^{19}$	$1.3 \times 10^1$
1	$3.5 \times 10^2$	$3.1 \times 10^2$	$1.8 \times 10^{20}$	$1.1 \times 10^1$
2	$5.5 \times 10^2$	$5.0 \times 10^2$	$3.8 \times 10^{20}$	8.2
4	$9.6 \times 10^2$	$9.6 \times 10^2$	$8.7 \times 10^{20}$	6.9
6	$1.4 \times 10^3$	$1.2 \times 10^3$	$1.4 \times 10^{21}$	5.1

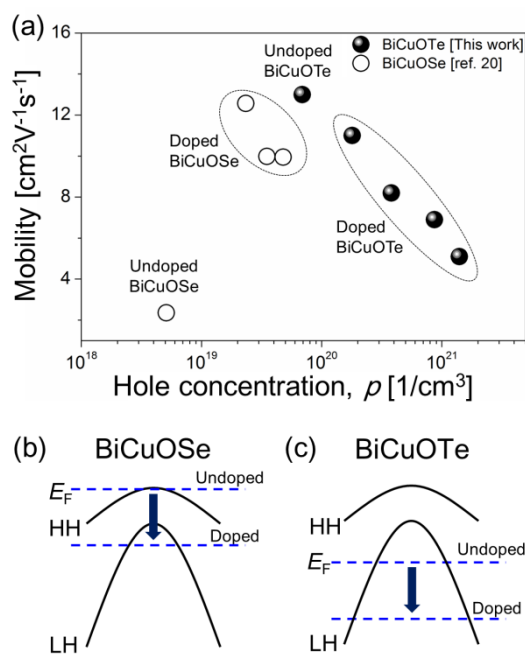


Fig. 3(a) Mobilities of the Bi<sub>1-x</sub>Pb<sub>x</sub>CuOTe compounds as a function of carrier concentration at room temperature. (b) and (c) are schematics of the two band structure in BiCuOSe and BiCuOTe, respectively. (HH: heavy hole, LH: light hole, E<sub>F</sub>: Fermi level)

In this experiment, even the undoped BiCuOTe exhibited degenerately doped conducting behaviour due to the native point defects and its mobility was considerably high ( $1.3 \times 10^4$  cm<sup>2</sup>V<sup>-1</sup>s<sup>-1</sup>). Therefore, it demonstrates that the charge transport in BiCuOTe is governed by the light-hole band as depicted in Figure 3(c), and the decrease in the mobility by Pb-doping is influenced by the ionized impurity scattering as reported in our previous work.<sup>20</sup>

Based on the DFT calculations, the formation energies of possible point defects were calculated to understand the detailed doping mechanism, and the results are shown in Table 3. In order to describe formation energy, we consider 4×4×2 extended cell. We optimized the atomic positions of all considered systems on the basis of DFT calculations while keeping the cell parameters at those values found in the experimental structure. In undoped BiCuOTe, the formation energies of Cu and Bi vacancy were calculated to be 55 and 66 meV/formula unit (FU), respectively. Although both types of vacancy could contribute to the hole generation together due to their very low formation energies, the vacancy formation energy at Cu site was slightly lower than that of Bi site. Therefore, the *p*-type character in undoped BiCuOTe is mainly attributed to the formation of Cu vacancy. As the amount of Pb increases in BiCuOTe, both the vacancy formation energies in the Bi and Cu sites decrease, however, the decrease in the formation energy of V<sub>Bi</sub> is much steeper than that of V<sub>Cu</sub>. Because of large ionic size of Pb<sup>2+</sup>, Pb-doping causes a structural strain in the (Bi<sub>2</sub>O<sub>2</sub>)<sup>2+</sup> layer, and this strain can be alleviated by introducing Bi vacancy. As a consequence, Pb-doping in Bi site can trigger the generation of extra hole carrier

Table 3. DFT calculations of the formation energies of Bi and Cu vacancy in Bi<sub>1-x</sub>Pb<sub>x</sub>CuOTe.

Compound	Vacancy formation energy (meV/FU)	
	Bi vacancy	Cu vacancy
BiCuOTe	66	55
Bi <sub>0.985</sub> Pb <sub>0.015</sub> CuOTe	34	37
Bi <sub>0.97</sub> Pb <sub>0.03</sub> CuOTe	18	21
Bi <sub>0.955</sub> Pb <sub>0.045</sub> CuOTe	3	6
Bi <sub>0.94</sub> Pb <sub>0.06</sub> CuOTe	-10	-8

by reducing the formation energy of *p*-type point defects, especially V<sub>Bi</sub>, for the strain relaxation.

Figures 4(a) and (b) show the effects of Pb-doping on the Seebeck coefficient and power factor of the Bi<sub>1-x</sub>Pb<sub>x</sub>CuOTe compounds, respectively. As the Pb content increased in the compound, the Seebeck coefficient rapidly decreased due to the increase in the hole concentration through the anomalous doping mechanism. Consequently, significant enhancement of the power factor could not be achieved by Pb-doping in this experiment. When  $x \geq 0.4$ , the Seebeck coefficients were linearly proportional to temperature, indicating that the carrier concentrations in the compounds are almost constant in the temperature range used in this study. Meanwhile, the Seebeck coefficients of the compounds ( $x \leq 0.2$ ) deviated from the linearity at relatively high temperature due to the extrinsic-intrinsic transition. This result is quite consistent with the charge transport properties discussed in Figure 2(a).

The Seebeck coefficients at room temperature are plotted as a function of carrier concentration in Figure 4(c), and they were compared with the calculated Seebeck coefficients. In the inset, the Fermi energy level indicates that even the undoped BiCuOTe is degenerately doped at room temperature due to the native point defects. This result is also consistent with the temperature dependence of its electrical conductivity below the extrinsic-intrinsic temperature in Figure 2(a), and it exhibits the importance of the native point defects on the thermoelectric performance in this material system. Theoretically, Seebeck coefficients can be calculated by eq. (1) in the case of single parabolic band structure.<sup>29-31</sup> In this work, the charge transport in BiCuOTe is dominantly governed by a single band of light-hole regardless of Pb-doping as discussed above.

$$S = -\frac{k_B}{e} \left( \frac{(r+5/2)F_{r+3/2}(\xi)}{(r+3/2)F_{r+1/2}(\xi)} - \xi \right), \quad (1)$$

where  $k_B$  is Boltzmann constant,  $e$  is electron charge,  $r$  is scattering parameter (+1/2 for optical phonon scattering, -1/2 for acoustic phonon scattering and +3/2 for ionized impurity scattering),  $F_n$  is Fermi integral in Eq. (2), and  $\xi$  is reduced Fermi energy in Eq. (3).

$$F_n = \int_0^{\infty} \frac{x^n}{1 + \exp(x - \xi)} dx, \quad (2)$$

$$\xi = \frac{E_V - E_F}{k_B T}, \quad (3)$$

where  $E_V - E_F$  is the Fermi energy level with respect to the top of the valence band. For the calculation, effective mass was treated as a free parameter.

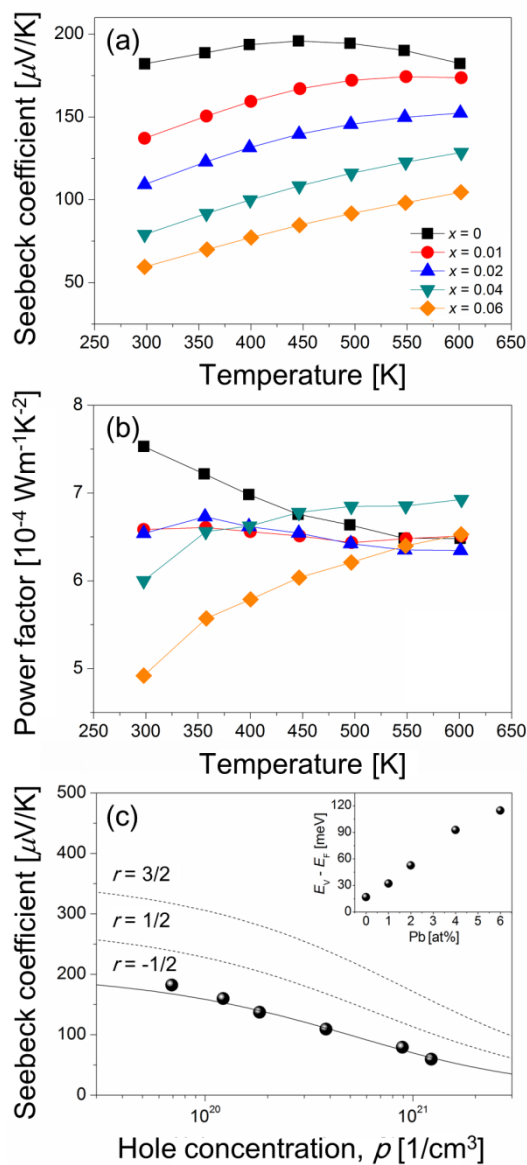


Fig. 4 (a) Temperature-dependent Seebeck coefficients and (b) power factors of the  $\text{Bi}_{1-x}\text{Pb}_x\text{CuOTe}$  compounds. (c) Carrier concentration-dependent Seebeck coefficients of the  $\text{Bi}_{1-x}\text{Pb}_x\text{CuOTe}$  compounds at room temperature and calculated Seebeck coefficients (solid line:  $r = -1/2$ , dashed line:  $r = 1/2$  and  $3/2$ ). Calculated Fermi energy levels ( $E_V - E_F$ ) are shown in the inset.

As shown in Figure 4(a), the calculated Seebeck coefficients based on the acoustic phonon scattering model ( $r = -1/2$ ) are

well fitted to the experimental values, implying that the degree of non-parabolicity in  $\text{BiCuOTe}$  could be negligible for the calculation using eq. (1). This result is consistent not only with the previous reports in doped  $\text{BiCuOSe}$  compounds,<sup>12,16,32</sup> but also with the observed scattering mechanism for the electrical conductivity ( $\sigma \propto T^{-1.5}$ ) in Figure 2(a).

Figures 5(a) and (b) show thermal conductivities and resulting  $ZT$  values of the  $\text{Bi}_{1-x}\text{Pb}_x\text{CuOTe}$  compounds, respectively. Undoped  $\text{BiCuOTe}$  compound exhibited a quite low thermal conductivity ( $0.834 \text{Wm}^{-1}\text{K}^{-1}$  at room temperature). The thermal conductivity increased with the increase in the amount of Pb-doping, and it could be explained by the increased electrical contribution to the thermal conductivity. When  $x \geq 0.4$ , the thermal conductivity monotonously decreased with increasing temperature. However, in the case of  $x \leq 0.02$ , there was a transition in its temperature dependence of the thermal conductivity at around  $450 \sim 500\text{K}$  due to the onset of the bipolar conduction. This behaviour is considerably consistent with the results of the charge transport in Figure 2(a) and also the Seebeck coefficient in Figure 4(a). Eventually, the  $ZT$  values decreased monotonically with the increase in the amount of Pb and the highest  $ZT$  value (0.51 at  $600\text{K}$ ) was obtained in undoped  $\text{BiCuOTe}$  compound.

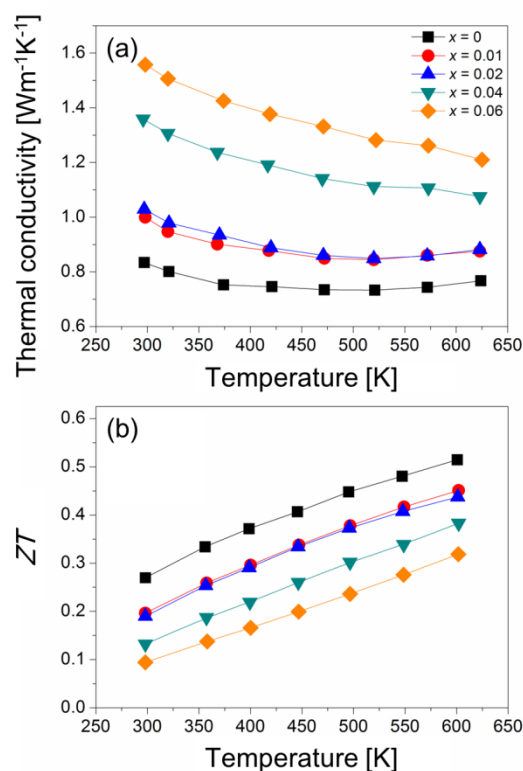


Fig. 5 (a) Temperature-dependent thermal conductivities and  $ZT$  values of the  $\text{Bi}_{1-x}\text{Pb}_x\text{CuOTe}$  compounds.

## Conclusions

In summary, point defect-assisted doping mechanism and related thermoelectric properties in Pb-doped BiCuOTe compounds were investigated. Degenerately doped *p*-type semiconducting behaviour was observed even in undoped BiCuOTe due to the native point defects, and the formation of the point defect was accelerated by the substitution of Bi with Pb. DFT calculations demonstrated that Pb-doping leads to the generation of extra charge carrier by reducing the formation energy of  $V_{\text{Bi}}$  for the strain relaxation which resulting from the larger ionic radius of  $\text{Pb}^{2+}$  than  $\text{Bi}^{3+}$ . The electrical conductivity in Pb-doped BiCuOTe could be significantly enhanced due to the unexpected increase of hole concentration, while it led to the drastic decrease in Seebeck coefficient. Therefore, the point defect-assisted doping in the  $\text{Bi}_{1-x}\text{Pb}_x\text{CuOTe}$  compounds inevitably entailed the increase in thermal conductivity, consequently leading to the decrease in *ZT*. With these results, it can be concluded that thermoelectric performance of BiCuOTe compound is critically determined by the native point defects, and that finding a suitable donor to compensate the holes can be a possible way to improve the thermoelectric performance.

## Acknowledgements

This research was supported by Nano-Material Technology Development Program (2011-0030147) through the National Research Foundation of Korea (NRF) funded by the Ministry of Education, Science and Technology, and also supported by the Dual Use Technology Program (12-DU-MP-01) of the Agency for Defense Development, Republic of Korea.

## Notes and references

<sup>a</sup>Energy and Environmental Division, Korea Institute of Ceramic Engineering and Technology, Seoul 153-801, Republic of Korea. E-mail: yslim@kicet.re.kr

<sup>b</sup>Department of Materials Science and Engineering, Seoul National University, Seoul 151-744, Republic of Korea. E-mail: pchan@snu.ac.kr

<sup>c</sup>LG Chem/Research Park, Daejeon 305-380, Republic of Korea

<sup>d</sup>Department of Chemistry, Pohang University of Science and Technology, Pohang 790-784, Korea. E-mail: jhshim@postech.ac.kr

<sup>e</sup>Divisions of Advanced Nuclear Engineering, Pohang University of Science and Technology, Pohang 790-784, Korea

Electronic supplementary information (ESI) available: XRD peak-to-peak height between  $\text{Bi}_2\text{O}_3$  and BiCuOTe and standard deviations of the lattice parameters of  $\text{Bi}_{1-x}\text{Pb}_x\text{CuOTe}$  compounds. See DOI: 10.1039/b000000x/

1 M. Palazzi, *C. R. Acad. Sci. Paris*, 1981, **292**, 789.

2 W. J. Zhu, Y. Z. Huang, C. Dong, and Z. X. Zhao, *Mater. Res. Bull.*, 1994, **29**, 143.

3 B. A. Popovkin, A. M. Kusainova, V. A. Dolgikh, and L. G. Aksel'rud, *Russ. J. Inorg. Chem.*, 1998, **43**, 1471.

4 J. Li, J. Sui, Y. Pei, C. Barreteau, D. Berardan, N. Dragoe, W. Cai, J. He, and L. D. Zhao, *Energy Environ. Sci.*, 2012, **5**, 8543.

5 F. Li, T.-R. Wei, F. Kang, and J.-F. Li, *J. Mater. Chem. A*, 2013, **1**, 11942.

6 J. Li, J. Sui, C. Barreteau, D. Berardan, N. Dragoe, W. Cai, Y. Pei, and L.-D. Zhao, *J. Alloy. Compd.*, 2013, **551**, 649.

7 S. Inoue, K. Ueda, H. Hosono, and N. Hamada, *Phys. Rev. B*, 2011, **64**, 245211.

8 H. Sato, H. Negishi, A. Wada, A. Ino, S. Negishi, C. Hirai, H. Namatame, M. Taniguchi, K. Takase, Y. Takahashi, T. Shimizu, Y. Takano, and K. Sekizawa, *Phys. Rev. B*, 2003, **68**, 035112.

9 K. Ueda, H. Hiramatsu, H. Ohta, M. Hirano, T. Kamiya, and H. Hosono, *Phys. Rev. B*, 2004, **69**, 155305.

10 K. Ueda, H. Hosono, and N. Hamada, *J. Appl. Phys.*, 2005, **98**, 043506.

11 H. Hiramatsu, H. Yanagi, T. Kamiya, K. Ueda, M. Hirano, and H. Hosono, *Chem. Mater.*, 2008, **20**, 326.

12 J. L. Lan, B. Zhan, Y. C. Liu, B. Zheng, Y. Liu, Y. H. Lin, and C. W. Nan, *Appl. Phys. Lett.*, 2013, **102**, 123905.

13 Y. L. Pei, J. He, J. F. Li, F. Li, Q. Liu, W. Pan, C. Barreteau, D. Berardan, N. Dragoe, and L. D. Zhao, *NPG Asia Mater.*, 2013, **5**, e47.

14 L. D. Zhao, D. Berardan, Y. L. Pei, C. Byl, L. Pinsard-Gaudart, and N. Dragoe, *Appl. Phys. Lett.*, 2010, **97**, 092118.

15 J. Sui, J. Li, J. He, Y. L. Pei, D. Berardan, H. Wu, N. Dragoe, W. Cai, and L. D. Zhao, *Energy Environ. Sci.*, 2013, **6**, 2916.

16 L. Pan, D. Berardan, L. Zhao, C. Barreteau, and N. Dragoe, *Appl. Phys. Lett.*, 2013, **102**, 023902.

17 S. D. N. Luu, and P. Vaquero, *J. Mater. Chem. A*, 2013, **1**, 12270.

18 J.-L. Lan, Y.-C. Liu, B. Zhan, Y.-H. Lin, B. Zhang, X. Yuan, W. Zhang, W. Xu, and C.-W. Nan, *Adv. Mater.*, 2013, **25**, 5086.

19 J. Li, J. Sui, Y. Pei, X. Meng, D. Berardan, N. Dragoe, W. Cai, and L.-D. Zhao, *J. Mater. Chem. A*, 2014, **2**, 4903.

20 D. S. Lee, T.-H. An, M. Jeong, H.-S. Choi, Y. S. Lim, W.-S. Seo, C.-H. Park, C. Park, and H.-H. Park, *Appl. Phys. Lett.*, 2013, **103**, 232110.

21 G. Rogl, A. Grytsiv, P. Rogl, E. Bauer, M.B. Kerber, M. Zehetbauer, and S. Puchegger, *Intermetallics*, 2010, **18**, 2435.

22 D. Zou, S. Xie, Y. Liu, J. Lin, and J. Li, *J. Mater. Chem. A*, 2013, **1**, 8888.

23 P. Vaquero, G. Guelou, M. Stec, E. Guilmeau and A. V. Powell, *J. Mater. Chem. A*, 2013, **1**, 520.

24 P. E. Blöchl, *Phys. Rev. B*, 1994, **50**, 17953.

25 G. Kresse and D. Joubert, *Phys. Rev. B*, 1999, **59**, 1758.

26 G. Kresse and J. Furthmüller, *Phys. Rev. B*, 1996, **54**, 11169.

27 J. P. Perdew, K. Burke and M. Ernzerhof, *Phys. Rev. Lett.*, 1996, **77**, 3865.

28 D. Shannon, *Acta Crystallogr.*, 1976, **32**, 751.

29 D. L. Young, T. J. Coutts, V. I. Kaydanov, A. S. Gilmore, and W. P. Mulligan, *J. Vac. Sci. Technol. A*, 2000, **18**, 2978.

30 A.F. May, E. S. Toberer, A. Saramat, and G. J. Snyder, *Phys. Rev. B*, 2009, **80**, 125205.

31 P. Jood, R. J. Mehta, Y. Zhang, G. Peleckis, X. Wang, R. W. Siegel, T. Borca-Tasciuc, S. X. Dou, and G. Ramanath, *Nano Lett.*, 2011, **11**, 4337.

32 C. Barreteau, D. Berardan, E. Amzallag, L. D. Zhao, and N. Dragoe, *Chem. Mater.* 2012, **24**, 3168.